Atmos. Chem. Phys., 10, 2079–2089, 2010
www.atmos-chem-phys.net/10/2079/2010/

Atmospheric Chemistry and Physics

MAX-DOAS measurements in southern China: retrieval of aerosol extinctions and validation using ground-based in-situ data

X. Li[1,2], T. Brauers[2], M. Shao[1], R. M. Garland[3], T. Wagner[4], T. Deutschmann[5], and A. Wahner[2]

[1]College of Environmental Sciences and Engineering, Peking University, Beijing, China
[2]Institute for Chemistry and Dynamics of the Geosphere (ICG-2), Forschungszentrum Jülich, Germany
[3]Biogeochemistry Department, Max Planck Institute for Chemistry, Mainz, Germany
[4]Satellite Group, Max Planck Institute for Chemistry, Mainz, Germany
[5]Institute for Environmental Physics, Universität Heidelberg, Heidelberg, Germany

Received: 25 July 2008 – Published in Atmos. Chem. Phys. Discuss.: 29 September 2008
Revised: 12 January 2010 – Accepted: 8 February 2010 – Published: 1 March 2010

Abstract. We performed MAX-DOAS measurements during the PRiDe-PRD2006 campaign in the Pearl River Delta region 50 km north of Guangzhou, China, for 4 weeks in June 2006. We used an instrument sampling at 7 different elevation angles between 3° and 90°. During 9 cloud-free days, differential slant column densities (DSCDs) of O_4 (O_2 dimer) absorptions between 351 nm and 389 nm were evaluated for 6 elevation angles. Here, we show that radiative transfer modeling of the DSCDS can be used to retrieve the aerosol extinction and the height of the boundary layer. A comparison of the aerosol extinction with simultaneously recorded, ground based nephelometer data shows excellent agreement.

1 Introduction

Differential Optical Absorption Spectroscopy (DOAS) is a powerful technique for the measurement of (see Platt and Stutz, 2008, and references therein). Multi-AXis Differential Optical Absorption Spectroscopy (MAX-DOAS) is a relatively new technique, which was recently developed (Hönninger et al., 2004) and was first used to retrieve bromine oxide in the troposphere (Hönninger and Platt, 2002). The MAX-DOAS technique was successfully used by different groups in order to measure NO_2 (e.g. Leigh et al., 2007; Pikelnaya et al., 2007), HCHO (e.g. Inomata et al., 2008), CHOCHO (e.g. Sinreich et al., 2007), and other uv or vis light absorbing molecules. Moreover, Wagner et al. (2004) developed a technique to use the O_4 absorption to retrieve aerosol extinctions (cf. Wittrock et al., 2004; Friess et al., 2006; Irie et al., 2008; Lee et al., 2009).

The general idea of MAX-DOAS is to record spectra of scattered sunlight at different elevation angles, α (i.e. the angle between the viewing direction of the telescope and the horizontal direction). For an individual measurement at elevation angle α, the measured optical density refers to the slant column density (SCD), which is the concentration $C(s)$ of a species integrated along the paths s where the photons traveled

$$\mathrm{SCD}_\alpha = \int C(s)ds = \frac{1}{\sigma}\log\left(\frac{I_0}{I_\alpha}\right) \quad (1)$$

Here σ is the absorption cross section, I_0 is the reference spectrum, and I_α is the measured spectrum. Since the SCD strongly depends on the observation geometry and meteorological conditions, it is usually converted to vertical column density (VCD). The conversion from SCD to VCD is achieved by the air mass factor (AMF), i.e. the averaged light path enhancement for solar light traveling through the atmosphere compared to a straight vertical path (cf. Platt and Stutz, 2008).

For measurements focusing on the species in the troposphere, differential slant column densities (DSCDs) are widely used (e.g. Irie et al., 2008; Pikelnaya et al., 2007). The DSCD is the difference between the SCDs at $\alpha \neq 90°$ and α=90°.

$$\mathrm{DSCD}_\alpha = \mathrm{SCD}_\alpha - \mathrm{SCD}_{90°} = \frac{1}{\sigma}\log\left(\frac{I_{90°}}{I_\alpha}\right) \quad (2)$$

During the analysis of MAX-DOAS measurement, the DSCD can be directly retrieved by using the spectrum taken at α=90° of each measurement cycle as reference spectrum in the DOAS fit. For both, $I_{90°}$ and I_α, the light paths in the

Correspondence to: T. Brauers
(th.brauers@fz-juelich.de)

stratosphere are nearly identical. Thus, the contribution of trace gas absorption in the stratosphere nearly vanishes.

MAX-DOAS instruments can be very simple and easy to operate. They require a (small) telescope that can be directed to several directions in the sky, including the zenith. The second component is a spectrograph with a typical DOAS resolution of 0.1 nm to 1 nm. However, despite the simplicity of the experimental setup, the evaluation of MAX-DOAS measurements from measured spectra to aerosol and trace gas concentrations or profiles is a demanding task. This evaluation requires the use of radiative transfer modeling (RTM) especially for conditions when aerosol loads are high and multiple scattering occurs.

RTMs calculate the photon flux at a certain location (longitude, latitude, altitude) in the atmosphere depending on viewing direction, the solar position (zenith and azimuth angle) and a number of parameters describing absorption and scattering of photons on their way through the atmosphere. Besides clouds, the major influence on the photon paths has the distribution of aerosol in the troposphere especially in polluted areas. In this study we concentrate on the effect of aerosols and investigate only measurements under mostly cloud free conditions. Over the last years, different radiative transfer models have been developed (see Wagner et al., 2007, and references therein). We used McArtim (Deutschmann, 2009), which is a backward Monte-Carlo model.

RTMs were reviewed by Hendrick et al. (2006) and Wagner et al. (2007). Different RTMs differ in the way of simulating photon transverse process in the atmosphere, the treatment of the Earth's sphericity, the way of considering aerosol scattering, the inclusion of the photo-enhancement of short lifetime species, etc. Intercomparison activities demonstrate an agreement within 10% of simulated SCD and AMF of species like NO_2 and HCHO (Hendrick et al., 2006; Wagner et al., 2007). McArtim was compared intensively to Tracy-II, one of the participants in the comparison by Wagner et al. (2007) and was found to agree excellently (Deutschmann, 2009). The advantage of McArtim over Tracy-II is the improved computational speed and the increased number of output parameters.

The concept of aerosol retrieval from the oxygen dimer absorption was introduced by Wagner et al. (2004). The O_4 concentration is proportional to the square of O_2 concentration, and it mainly depends on the temperature and pressure profile. Since most of the O_4 resides in the lower part of the troposphere, the O_4 DSCD is sensitive to changes in the photon paths, mainly at low altitudes. Aerosol particles lead to a variation of photon paths and thus a variation in the O_4 DSCDs. Therefore, the O_4 DSCD can be used as an indicator of the aerosol load in the atmosphere. For conditions of low aerosol load or the existence of clouds, the probability of multiple scattering increases, which will lead to the simultaneous increase of the O_4 DSCDs at all elevation angles. Under conditions of high aerosol load, the distance from which photons can reach the telescope will strongly decrease due to the high aerosol extinction. This will cause a strong reduction of O_4 DSCDs especially those measured at low elevation angles. The high aerosol extinction also shortens the penetration depth of the incident sunlight, which is reflected by the decrease of the amplitude of O_4 DSCDs diurnal variation. A detailed sensitivity study on various parameters was performed by Wagner et al. (2004).

In this paper we use the oxygen dimer absorptions in the near uv to explore the aerosol layer at a semi-urban location in southern China. We have developed an automated method to retrieve the aerosol extinction and the height of the boundary layer from the measured O_4 DSCDs. The determination of the aerosol extinction was compared to ground-based, insitu measurements by a nephelometer. In a forthcoming paper we will explore the trace gas absorptions.

2 Experimental

2.1 The MAX-DOAS instrument

The instrument is a Mini-MAX-DOAS (Fa. Hoffmann, Rauenberg, Germany). It containes a miniature crossed Czerny-Tuner spectrometer unit USB2000 (Ocean Optics Inc.) with a spectral resolution of $\approx$0.7 nm full width at half maximum (FWHM). The spectral range of 292 nm to 443 nm is mapped onto a one-dimensional CCD-detector with 2048 pixels. The spectrometer unit was cooled to a stable temperature of +19 °C in order to minimize changes in optical properties of the spectrometer and to reduce detector dark current. The scattered sunlight was collected and focused by a quartz lens and was led into the spectrometer unit by a quartz fibre bundle. A stepper motor enabled the adjustment of the viewing direction to a desired elevation angle. All functions were controlled by a laptop via USB connection.

The instrument was operated by a fully automated measurement program (MiniMax, Udo Friess, University of Heidelberg). The program employed routines to adapt the integration time of the measurements to the light conditions in order to achieve a constant signal level (i.e. 80% of the saturation of the CCD-detector), to store the spectra and to control the movements of the telescope. The instrument slit function was determined by measuring the emission line of a mercury lamp at 334 nm. Scattered sunlight spectra were acquired sequentially at elevation angles of 90° (i.e. zenith), 30°, 20°, 15°, 10°, 5°, and 3°. One measurement cycle took 10 min to 15 min. The dark current and offset spectra were recorded every night.

2.2 The DOAS analysis

The O_4 DSCDs were determined by a DOAS fit in the wavelength range between 351 nm and 389 nm. The logarithm of a Fraunhofer reference spectrum (FRS), several trace gas absorption cross sections, a Ring spectrum (Grainger and Ring,

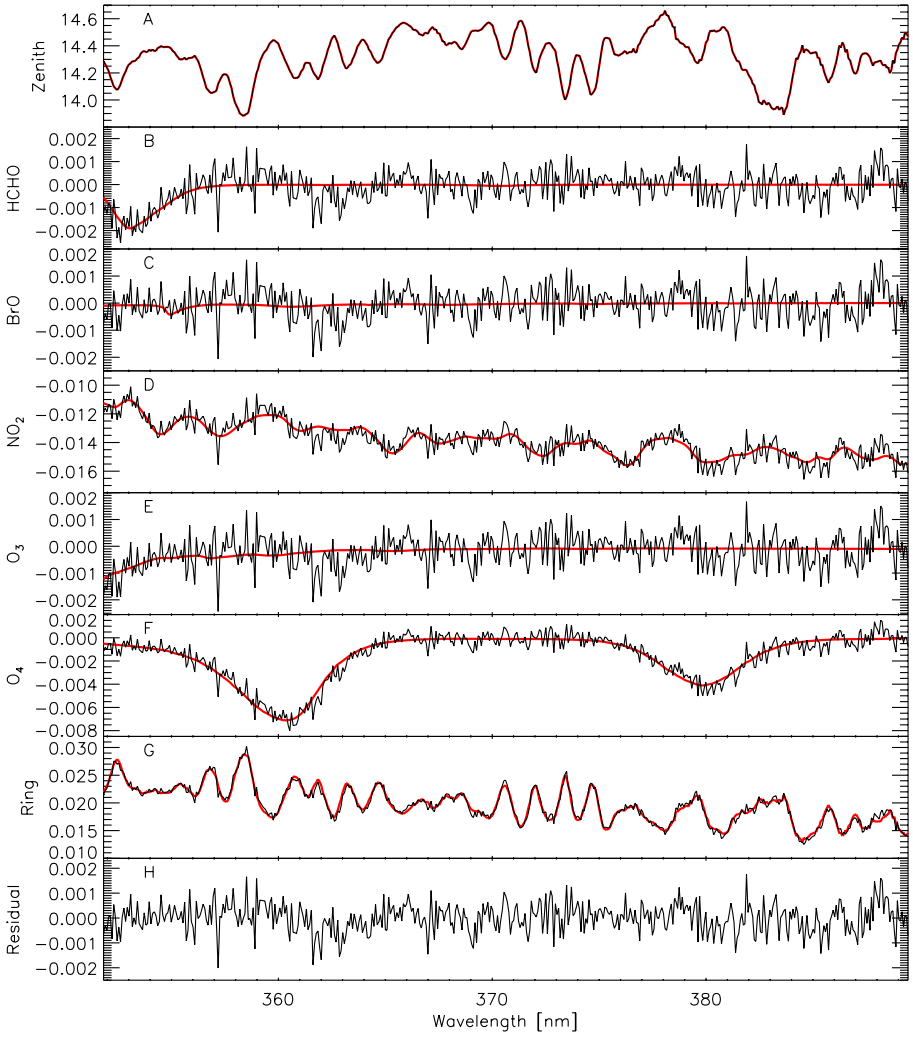

Fig. 1. Evaluation of a single spectrum (α=3°) recorded in the wavelength range 352 nm to 390 nm used for the O_4 determination on 19 July 2006 at 10:59. **(A)** Overlay of spectrum at 3° with fitted zenith spectrum. **(B), (C), (D), (E), (F)** Fitted HCHO, BrO, NO_2, O_3, and O_4 reference spectrum overlayed to the residual including the absorption.

1962), a third order polynomial and a second order offset polynomial were fitted together to the logarithm of the measured spectrum, which was already corrected for dark current and offset. During the fit, the measurement spectrum was allowed to shift and squeeze with respect to the FRS, the Ring spectrum and the absorption cross sections. The fitting procedure was conducted using the script mode of the DOASIS software (Kraus and Geyer, 2001).

Figure 1 illustrates one example of the DOAS fit recorded on 19 July 2006 at 10:59 at a solar zenith angle of 23° and an elevation angle of 3°. For each measurement cycle, the corresponding zenith spectrum (α=90°) was taken as FRS for the spectra at off-axis elevation angles. This largely eliminates the stratospheric contributions to the DSCDs. However, the O_4 DSCD is only marginally affected by stratospheric absorptions since O_4 mainly resides in the troposphere. The Ring spectrum was calculated from each measured spectrum (Bussemer, 1993). For the fit of the absorbing trace gases, we used high resolution absorption cross sections which were convolved by the instrument slit function to match the resolution of the instrument (except for the O_4 spectrum, which was interpolated). These references include HCHO (Meller and Moortgat, 2000), BrO (Wilmouth et al., 1999), NO_2 (Voigt et al., 2002), O_3 at 280 K (Voigt et al., 2001), and O_4 (Greenblatt et al., 1990) with manual adjustments of the wavelength axis (R. Sinreich, personal communication).

In addition, the solar I_0-effect (Platt et al., 1997) was corrected for NO_2 and O_3 reference spectra with slant column density of 1.5×10^{17} cm^{-2} and 1.5×10^{20} cm^{-2}, respectively. This correction was maximum 2% for the DSCDs. The wavelength calibration was performed by fitting the Fraunhofer reference spectra to a high resolution Fraunhofer

spectrum (Kurucz et al., 1984), convoluted with the instrument's slit function.

2.3 Setup of the instruments at the Guangzhou Backgarden supersite

The MAX-DOAS observations were performed in the framework of the "Program of Regional Integrated Experiments of Air Quality over the Pearl River Delta" (PRIDE-PRD2006; Hofzumahaus et al., 2009; Zhang et al., 2010). The intensive campaign took place from 3 July 2006 to 31 July 2006 in the Pearl River delta area in southern China. Our measurements were conducted in Backgarden (BG) supersite (23.50° N, 113.03° E). The Mini-MAX-DOAS device was installed on the top of a 10 m high hotel building, pointing to the east. The measurements were accompanied by a comprehensive suite of atmospheric measurements. In this study we used the data of a nephelometer and a photoacoustic spectrometer, which are described in a separate paper (Garland et al., 2008) and therefore only a brief description follows.

The total aerosol particle scattering coefficients and hemispheric backscattering coefficients at three different wavelengths (λ=450 nm, 550 nm, and 700 nm) were measured with an integrating nephelometer (Model 3563, TSI). The aerosol particle absorption coefficient at 532 nm was determined with a photoacoustic spectrometer (PAS; Desert Research Institute), which provides highly sensitive absorption measurements without interference by scattering signals (Arnott et al., 1999). The optical data were averaged for two minutes. The main aerosol inlet used for both instruments in this study was equipped with a PM_{10} inlet and a diffusion dryer with silica gel/molecular sieve cartridges (average sampling relative humidity 33%). The uncertainty (accuracy and precision) of the nephelometer and the PAS data are less than $\pm$10% (Garland et al., 2008).

3 Radiative transfer modelling and the retrieval of the aerosol extinction

The modeling of the O_4 DSCDs was performed by a backward Monte-Carlo approach with the treatment of multiple scattering in a fully spherical geometry, i.e. McArtim (Deutschmann, 2009). In this model, a photon emerges from a detector in an arbitrary line of sight direction and is tracked along the path in backward direction until the photon leaves the top of the atmosphere or is absorbed. The various events which may happen to the photon at various altitudes are defined by suitable probability distributions. Random numbers decide on the occurrence of events. At each scatter event a weight is calculated from the product of two terms. The first factor is the probability that the sunlight reaches the scatter event, the second is the phase function of the scatter event evaluated at the angle between the Sun direction and the direction of the sampled trajectory from the scatter event to the detector. For each trajectory an estimate of the normalized sun radiance is obtained by adding the weights of all scatter orders. A large number of random photon paths are generated, thus reproducing the light contributing to the simulated measurement.

The McArtim model requires a number of input parameters like altitude, solar zenith and azimuth angles, pressure, temperature, concentration of absorbing trace gases, and aerosol optical parameters for each layer in the atmosphere. The layers can be prescribed by the users. In the model runs we calculated the O_4 altitude profile from the square of the O_2 profile of the US standard atmosphere. We also used the temperature, pressure, and trace gas profiles from the US standard atmosphere. However, these parameters are of minor importance for the O_4 columns evaluated here. The major influence comes from the aerosol optical parameters and the aerosol altitude profile.

For the aerosol optical properties, we selected a constant single scattering albedo (SSA) and a constant asymmetry parameter (g, under the Henyey-Greenstein approximation) of 0.85 and 0.68, respectively. These were deduced from the nephelometer and PAS measurements and they refer to the average in the time frame between 06:00 and 19:00 (local time) for all days. We also set the surface albedo constant to 7%, a value also used by Irie et al. (2008). The sensitivity on the albedo is small: doubling the albedo changes the modeled O_4 DSCDs by less than 5%. The sensitivities on the single scattering albedo and the asymmetry parameter are larger: 10% changes in SSA and g modify the modeled O_4 DSCDs by 10% and 17%, respectively. We used 0.3° for the field of view of the telescope which influence is small. Even at $\pm$0.1° the results change by less than 1%.

For the aerosol profile, we assumed two layers, i.e. the atmospheric boundary layer and the free troposphere, which can be described with a limited set of parameters. Since our measurements were conducted at six independent values of the elevation angle only, it is required that the profiles are parameterized with less than six parameters. Over source regions, it is assumed that the well mixed boundary layer fills with particles, which are emitted or photochemically formed, while in the layer aloft the aerosol content quickly decreases with height. Observations in Asia (e.g. Sasano, 1996; Ansmann et al., 2005; Chiang et al., 2007) obtained these kinds of profiles.

Thus, the extinction profile $E(z)$ was taken as two layers in the range from 0 km to 15 km

$$E(z) = \begin{cases} \tau \cdot F/H & z \le H \\ \beta \cdot \exp(-z/\xi) & z > H \end{cases} \quad (3)$$

where z is the height above ground. τ is the aerosol optical depth from ground to 15 km (i.e. in the entire troposphere) and F is the fraction of the total extinction τ in boundary layer. H is the height of the boundary layer, β is the normalizing constant for the exponential factor, and ξ is the scaling

Table 1. Parameters for Lookup table (LUT) generation. SZA: solar zenith angle. SRAA: solar relative azimuth angle. F: fraction of the total extinction residing in the boundary layer. SSA: single scattering albedo. g: asymmetry parameter. FOV: field of view of the telescope. τ: aerosol optical depth (see Eq. 3). H: height of the boundary layer. ξ: scaling height of aerosol extinction in the free troposphere. #: number of McArtim runs for the setup of the LUT.

param	unit	values
SZA	deg	80.92, 69.58, 55.88, 42.19, 28.65, 14.72, 4.02, 13.22, 26.86, 40.75, 54.29, 67.66, 80.05
SRAA	deg	−19.72, −15.43, −11.09, −7.12, −2.82, 3.25, 80.82, 175.33, 182.36, 186.63, 190.64, 194.67, 199.13
F		0.1–1.0 (interval: 0.1)
SSA		0.85
g		0.68
FOV	deg	0.3
τ		0.05, 0.15, 0.3, 0.6, 1.0, 1.5, 2.0, 2.5, 3.0, 3.5, 4.0, 4.5
H	km	0.1, 0.3, 0.5, 0.7, 1.0, 1.5
ξ	km	5.0
#		9360

height for the aerosol in the free troposphere. For the latter we used a constant value of 5 km. The results presented here are not sensitive to ξ since most of the aerosol extinction resides in the boundary layer. In order for τ being the integrated optical depth, $E(z)$ must obey the boundary condition

$$\int_{0\text{km}}^{15\text{km}} E(z)dz = \tau \tag{4}$$

which leads to a conditional equation for β.

$$\beta = \frac{(1-F)\cdot\tau}{\xi\cdot(e^{-H/\xi} - e^{-15\text{km}/\xi})} \tag{5}$$

We also introduce the extinction at ground level $E_0 = \tau \cdot F/H$ that can be compared to local, ground based measurements.

With this input, the McArtim program calculates the set of O_4 DSCD for the six elevation angles R_α within 15 min on a typical state-of-the-art PC when 200 000 photon paths are simulated at λ=360 nm, i.e. the wavelength of the major O_4 absorption. In order to optimize the input parameters of McArtim (τ, F, and H) we minimize

$$\chi^2(\tau, F, H) = \sum_{\alpha=3^\circ}^{30^\circ} \left(\frac{M_\alpha - R_\alpha(\tau, F, H)}{\sigma(M_\alpha)} \right)^2 \tag{6}$$

where R_α indicates the modeled data and M_α the measured data. The weighing is done by the statistical error of the measured data, $\sigma(M_\alpha)$. The iterative χ^2 minimization requires several hours to days for a single data point when the RTM is called in every iterative step. We therefore created a look-up table (LUT) that is used as input for the fitting procedure.

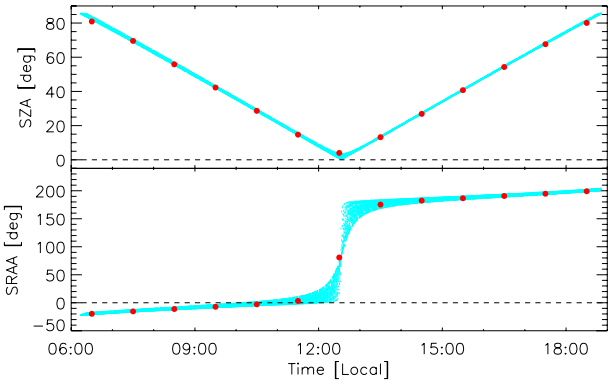

Fig. 2. Range of solar zenith angles and azimuth angles during the entire campaign. The blue symbols refer to the values of each single recorded spectrum, the red refer to the values used in the RTM calculation (see Table 1).

The LUT was based on a set of solar zenith angles, SZA, and relative azimuth angles, SRAA (see Table 1). These were not selected independently, since during the 4 week period they cover only a small band within the range of the possible values (Fig. 2). We also used single values for scattering albedo (SSA), asymmetry parameter (g), surface albedo, and scaling height (ξ) for the entire campaign. The range of the three free parameters were chosen to cover a wide range of possible situations in the LUTs for subsequent fitting. The number of required McArtim runs was 9360 corresponding to approximately 100 days of CPU time. However, this could be distributed to ≈30 PCs during off-time hours.

The LUT provides O_4 DSCDs, L_α, as a function of the elevation angle α (3°, 5°, 10°, 15°, 20°, and 30°) and of the parameters τ, F, and H. For one measured cycle of O_4 DSCDs, M_α, we fitted the linearly interpolated values $L_\alpha(\tau, F, H)$ of the LUT (as a approximation for the $R_\alpha(\tau, F, H)$ in Eq. 6). In order to reduce the atmospheric variations as well as measurement noise of a single observation, the profile retrieval was applied to measured O_4 DSCDs averaged over one hour. The minimization procedure was conducted automatically using the Levenberg-Marquardt algorithm (mpfit[1], realized in IDL). The errors of the retrieved parameters were derived from the fitting procedure.

4 Results and discussion

The MAX-DOAS instrument was operated for the most of the field campaign period from 3 July 2006 to 25 July 2006. However, since most days of the campaign

[1]C. B. Markwardt, mpfit – Robust non-linear least squares curve fitting, http://cow.physics.wisc.edu/~craigm/idl/fitting.html

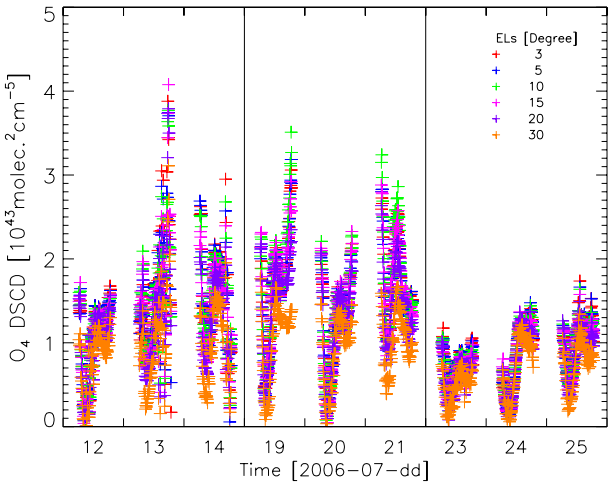

Fig. 3. Differential slant column densities of O_4 measured on cloud free days during the PRiDe PRD2006 campaign. Low values on 23–25 July 2006 refer to high aerosol loads close to the surface.

were characterized by clouds, we selected 9 virtually cloud-free days for this study on aerosols (Fig. 3). We see the influence of the elevation angle, the diurnal variation of the O_4 DSCD with the solar zenith angle and the effect of aerosols. Wagner et al. (2004) showed that aerosol particles close to the surface would reduce the difference of O_4 DSCDs between the different elevation angles as well as the magnitude of the O_4 DSCDs, providing a qualitative way to identify high aerosol load conditions. For example, the strong decrease of O_4 DSCDs in the last 3 days reflects the increase of aerosol load, also observed by in-situ measurements.

Figure 4 demonstrates two examples of the aerosol retrieval on 24 July 2006. The left column (Fig. 4a, c) shows the result for the time interval from 07:00–08:00. The best fit is reached when τ, F, and H are 3.22, 0.90, and 0.59 km, respectively. The right column (Fig. 4b, d) corresponds to 15:00–16:00 and a best fit at τ, F, and H are 1.03, 0.79, and 1.62 km, respectively. Based on τ, F, and H (their statistical 1-σ errors are given in Fig. 4c, d) we can calculated the aerosol extinction at the ground (E_0) as $4.91\pm1.96\,\mathrm{km}^{-1}$ and $0.50\pm0.04\,\mathrm{km}^{-1}$ for the two cases. Firstly, when the aerosol load is high and aerosols are concentrated in a shallow layer near the ground, the O_4 DSCDs at all elevation angles will decrease. The two times lower values of O_4 DSCDs in Fig. 4a compared to those in Fig. 4b reflects the difference of the aerosol distribution between the two time intervals. Secondly, as far as the error of E_0 is concerned, the larger error reflects the high aerosol extinction nearby, which leads to the low intensity of light received by the instrument and thus the large measurement error since the S/N ratio is reduced. Consequently, a larger error of E_0 can always be expected for early morning hours when the aerosol load was high. The O_4 DSCDs is dominated by the aerosol distribution near the ground-based instrument; the contribution from aerosols in upper layers is of minor importance. These results demonstrate the existence of high aerosol extinction in the layer near the ground.

In the retrieval processes, the aerosols in the lowest layer (i.e. 0–H) are assumed to be distributed homogeneously (see Eq. 3). Therefore, the retrieved aerosol extinction in this layer E_0 can be compared to the simultaneous in-situ, ground-based nephelometer measurements. The nephelometer detects the aerosol total scattering (T_S) which is the major part of the extinction of ambient aerosols in most cases. The total aerosol scattering at the O_4 absorption at the wavelength of the MAX-DOAS measurment is calculated by extrapolation. A second order polynomial was fitted to the measured total aerosol scattering at three different wavelengths and extrapolated to 360 nm (Eck et al., 1999). The comparison of E_0 against T_S will help us to validate the retrieval under the assumption of constant aerosol in the lowest layer.

Figure 5 illustrates the time series of the converted nephelometer reading T_S and E_0 derived from the MAX-DOAS. The absolute values as well as the diurnal variations of aerosol extinction are very similar. Large differences between T_S and E_0 mainly occur during morning hours. These can be attributed to several reasons:

– The nephelometer only records the scattered light from the aerosol, which is the larger part of the light loss in most cases. However, the simultaneous in-situ photoacoustic spectrometer measurements demonstrated that aerosol absorption during morning hours was high during most of the days.

– An overestimation of the SSA will cause an overestimation of aerosol extinction by MAX-DOAS O_4 observations. The SSA been used for the RTM was a constant value of 0.85. However, the measured SSA during the period when the discrepancies existed was usually lower than 0.85. Sensitivity tests showed that the decrease of SSA by 5 % will lead to a decrease of modeled O_4 DSCDs by ≈5%. In order to achieve the best fit between modeled and measured O_4 DSCDs, the retrieval procedure will increase the aerosol extinction to compensate for the higher value of SSA.

– The MAX-DOAS instrument was scanning towards east direction, thus more forward scattering is relevant for the measurements during sunrise. In order to access this effect we looked at the sensitivity on SSA and g in the morning and at noon. In the early morning (06:30), the sensitivities (δ(DSCD)/DSCD)/(δ(SSA)/SSA) and (δ(DSCD)/DSCD)/($\delta(g)/g$) are 2 and 3, respectively, compared to 1 and 1.5 around noon.

– Also small clouds or horizontal inhomogeneities caused by local emissions could cause differences between

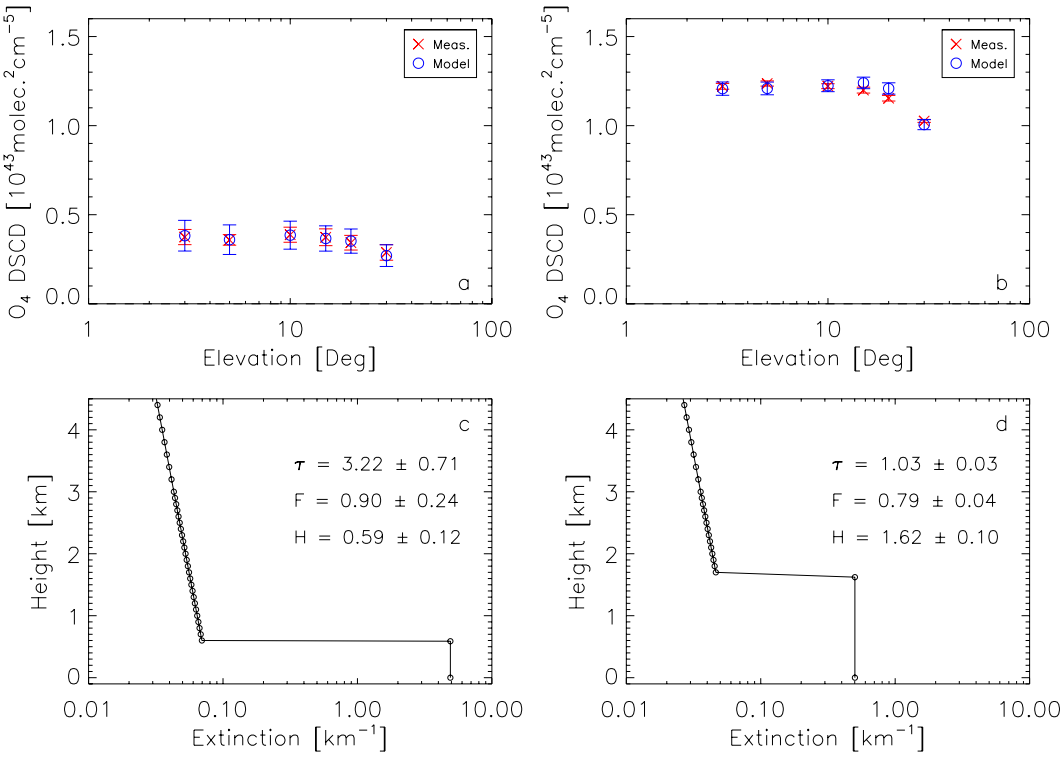

Fig. 4. Two examples for the retrieval of the aerosol extinction with different aerosol loads. Upper row: comparison of measured and modeled O_4 DSCDs. Lower row: retrieved profiles. The parameters indicate the optimized estimators and their 1-σ fitting errors. Left: 24 July 2006, 07:00–08:00, SZA=70°. Right: 24 July 2006, 15:00–16:00, SZA=41°.

MAX-DOAS and nephelometer. However, we selected the virtually cloud free days. In addition the high aerosol load reduced the visibility. Therefore, the sampling area of the MAX-DOAS was small and most likely not influenced by isolated local sources.

– The largest influence on the comparison between E_0 and T_S, however, may be the influence of humidity, e.g. the existence of fog in morning hours. The aerosol sampled by the nephelometer were first dried to ≈35% relative humidity. Therefore, the nephelometer is insensitive to changes in ambient relative humidity and the resulting impacts on the aerosol scattering. This is certainly not the case for MAX-DOAS observations, which were performed outside at ambient humidities between 55% and 99%. The higher values occurred in the morning hours. On the one side, the asymmetry parameter g and the single scattering albedo SSA of fog particles can be different from the values selected for the RTM calculation. On the other side, the aerosol growth with humidity. We corrected the aerosol scattering T_S using an empirical hygroscopic growth factor F based on the relative humidity rh.

$$T_S(\text{corr}) = T_S \times F(rh) = T_S \times (1 + a(rh)^b) \quad (7)$$

Here, the empirical factors were set to $a = 2.06$ and $b = 3.6$ as described by Liu et al. (2008) for urban aerosols. Their measurements were performed at the same time (July 2006) at a downtown Guangzhou location about 60 km south east from our site. The corrected data are also presented in Fig. 5. The agreement is strongly improved, e.g. on 23 and 24 July where the values of T_S are increased by a factor of 2 by the correction. After the correction an almost perfect agreement is reached.

Given the arguments discussed above the correlation of E_0 and T_S(corr) is good. Based on the full dataset (N=90) the correlation coefficient is 0.93 (Fig. 6a). If we restrict the data to the time between 11:00 and 19:00, when the correction is of smaller importance, the correlation coefficient is still 0.85 at N=54 (Fig. 6a). An linear regression line was performed on both sets using error weights in both coordinates. We used standard deviation of the 1-h averaged nephelometer data and the fitting errors of the for x and y weights, respectively. The slope of 0.83±0.04 and intercept (0.08±0.04) km^{-1} for the entire dataset and the slope of 0.85±0.05 and intercept (0.08±0.03) km^{-1} for the restricted set do not differ significantly. In both cases the scatter around the regression line is well represented by the statistical errors

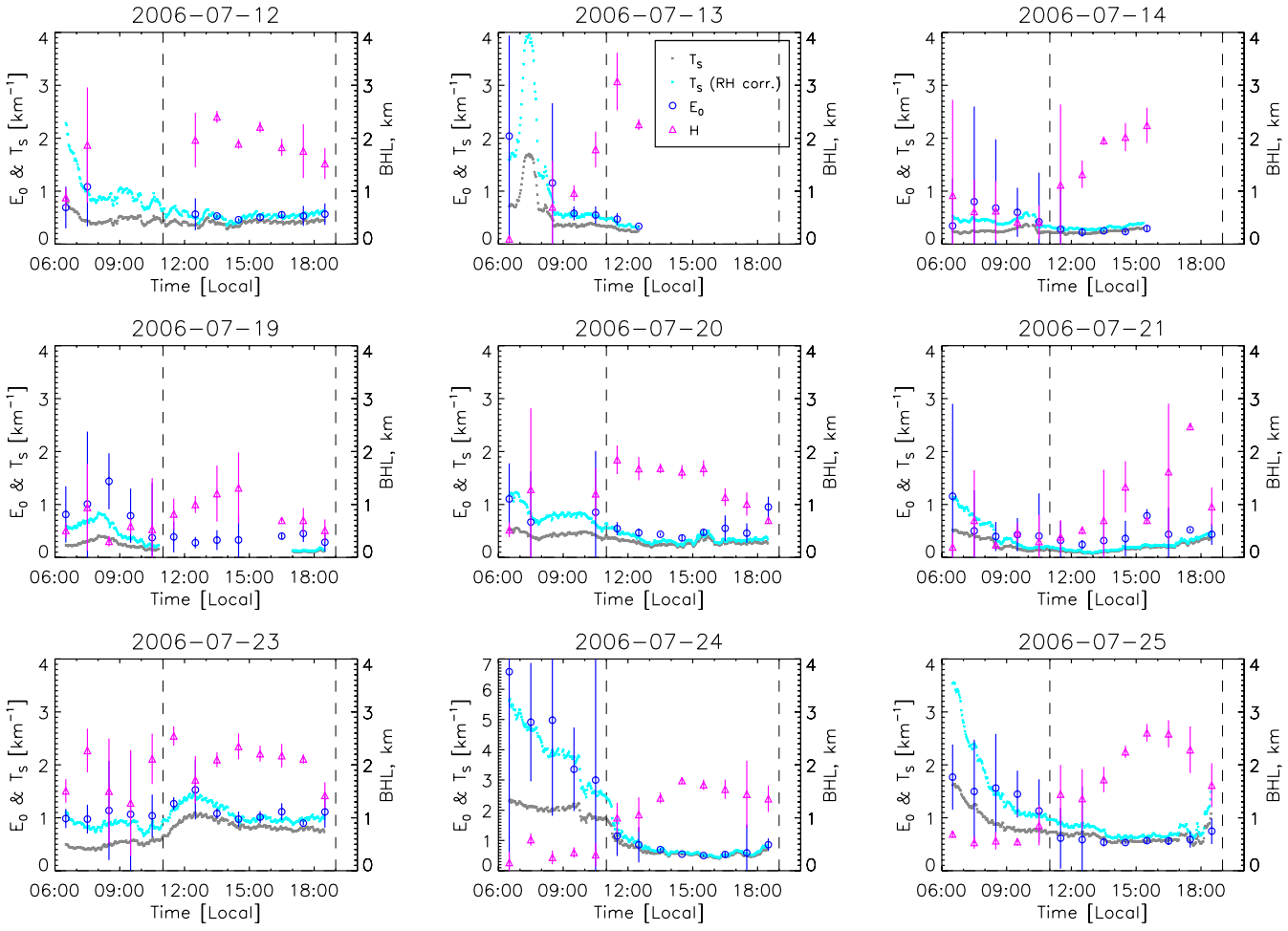

Fig. 5. Aerosol extinction E_0 and aerosol layer height H derived from MAX-DOAS measurements for 9 days during the PRD 2006 campaign. Also shown are the simultaneously recorded nephelometer readings, original and humidity corrected data. The dashed line indicates 11:00 the margin for data considered in Fig. 6b.

of both measurements. Considering the fact that the MAX-DOAS measures the aerosol extinction averaged over a distance while the nephelometer detects the aerosol scattering in the air mass near the instrument, the results of the linear regression demonstrate a good agreement between the measurement results of these two instruments. As described above, the major discrepancies between E_0 and T_S are found during morning hours.

We retrieved aerosol extinctions for all days plotted in Fig. 5. The variation of aerosol vertical distributions can be clearly identified: In the early morning hours (06:00–08:00), aerosols from fog and local emission processes were concentrated in a surface layer of approximately 800 m. With the sun rising and growing convection the height of the lowest layer, H, increased and aerosols in this layer dispersed to upper layers. Due to this mixing process, the aerosol extinction in the lowest layer started to decrease. The highest value of H accompanied the lowest value of the extinction in the afternoon (16:00–17:00). The decrease of H and the accumulation of aerosols in the lowest layer started again around sunset (18:00–19:00).

The diurnal cycle of H can be seen clearly from the single day shown in Fig. 5. However, the statistical error can be large and the values are variable when looking at one day only. Therefore, we accumulated all 9 days into one average diurnal profile (Fig. 7). The average mixing height was 0.7 km in early morning hours. It increased in the morning and reached the highest value of about 2 km in the afternoon. Unfortunately, the boundary layer was not independently measured. Thus no comparison can be presented here. The diurnal average aerosol extinction matches the humidity corrected nephelometer data for the entire day as already discussed for the correlations.

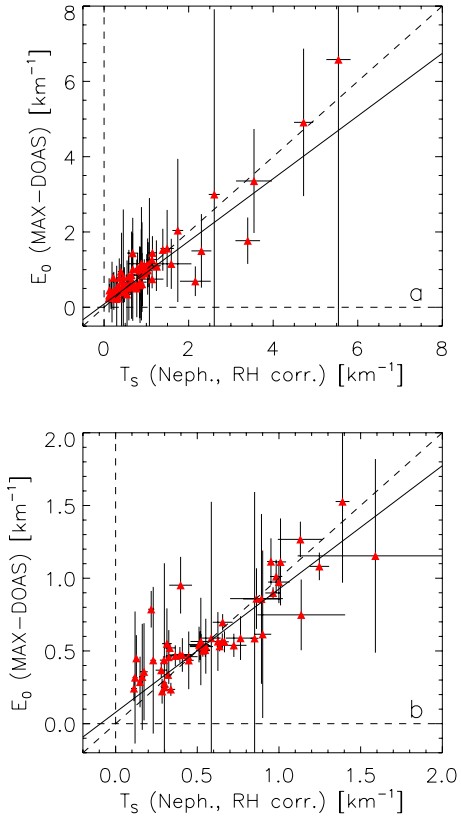

Fig. 6. Correlation and regression analysis of MAX-DOAS aerosol versus nephelometer data. **(a)** all data recorded during 9 days, **(b)** restricted to time interval 11:00 to 19:00. The dashed line corresponds to 1:1, the solid line corresponds to a linear fit (see text for details and retrieved slopes and intercepts).

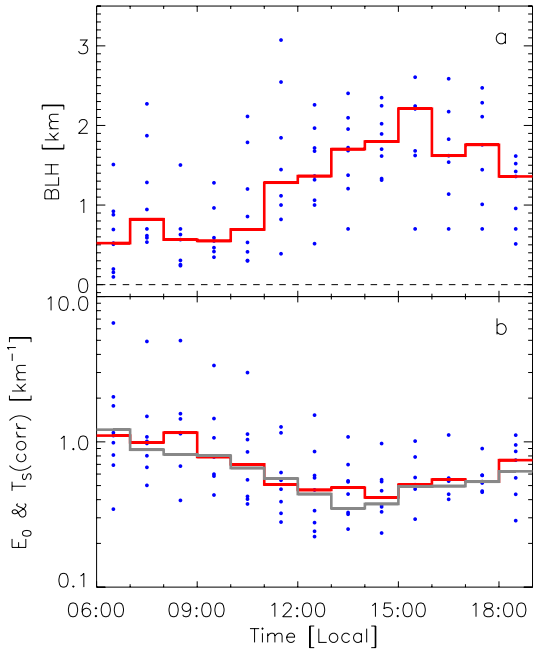

Fig. 7. Average diurnal profiles of aerosol layer height H and the aerosol extinction E_0. The blue dots correspond to the single measurement presented in Fig. 5, the red line to median within the 1-h time interval. **(a)** Aerosol layer height H. **(b)** Aerosol extinction E_0 and the nephelometer data (grey line) averaged over 1-h intervals.

5 Conclusions

In this study, the first MAX-DOAS measurements were performed in southern China. During a period of one month we encountered 9 days with no or marginal cloud cover. Under these conditions, we retrieved aerosol extinctions from the absorption features of the oxygen dimer, O_4, in the UV. The retrieval of the aerosol extinction and the aerosol boundary layer height was based on multi-parameter lookup-tables, which were created by the radiative transfer model McArtim. We minimized the difference between the measured and modeled O_4 differential slant column as a function of the viewing geometry, i.e. the elevation angle of the MAX-DOAS telescope.

Our lookup-table had 3 free parameters (the total aerosol extinction τ, the fraction of aerosol in the surface layer F, and the aerosol layer height H). Even at only 6 different elevation angles the fit of 3 free parameters was found to be meaningful for most conditions. This was shown by the good correlation with locally measured aerosol extinction, and the retrieval of reasonable aerosol/boundary layer heights between 500 m and 2 km.

The conditions at the Guangzhou backgarden supersite were mainly characterized by strong particulate pollution at ground level. The approach taken here assumed a constant single scattering albedo and asymmetry factor for the entire troposphere. This might not be adequate, even under conditions of high turbulence and mixing driven by an extremely high solar radiation. In addition, we had difficulties to constrain the total optical depth in some cases. These issues can be addressed by improving the lookup table setup and fitting strategy. However, this would require much more computing time for the RTM modeling and evaluation of sensitivities. For further experiments, we conclude that measured radiances can improve the evaluation process, as suggested by Friess et al. (2006). Furthermore, additional elevation and azimuth angles or the O_4 absorption at additional wavelengths can be measured and modeled to advance the quality of the aerosol profile retrieval from MAX-DOAS measurements.

Acknowledgements. The authors like to thank Roman Sinreich, Udo Friess, and Ulrich Platt (Heidelberg) for lending the Mini-MAX DOAS instrument, for the MiniMax software, and for fruitful discussions. The technical help and support at the field site from the PRiDe-PRD2006 campaign team, especially Rolf Häseler (Jülich), Min Hu, Limin Zeng, and Yuanhang Zhang (Beijing) are gratefully acknowledged. We thank all participants of the distributed computing of the RTM. This work was supported by the China National Basic Research and Development Program

2002CB410801, and the National High Technology Research and Development Program of China (863 Program) 2006AA06A301.

Edited by: M. van Roozendael

References

Ansmann, A., Engelmann, R., Althausen, D., Wandinger, U., Hu, M., Zhang, Y., and He, Q.: High aerosol load over the Pearl River Delta, China, observed with Raman lidar and Sun photometer, Geophys. Res. Lett., 32, L13815, doi:10.1029/2005GL023094, 2005.

Arnott, W. P., Moosmuller, H., Rogers, C. F., Jin, T. F., and Bruch, R.: Photoacoustic spectrometer for measuring light absorption by aerosol: instrument description, Atmos. Environ., 33, 2845–2852, doi:10.1016/S1352-2310(98)00361-6, 1999.

Bussemer, M.: Der Ring-Effekt: Ursachen und Einfluss auf die spektroskopische Messung stratosphäischer Spurenstoffe, Master's thesis, Universität Heidelberg, Germany, 1993.

Chiang, C.-W., Chen, W.-N., Liang, W.-A., Das, S. K., and Nee, J.-B.: Optical properties of tropospheric aerosols based on measurements of lidar, sun-photometer, and visibility at Chung-Li (25 N, 121 E), Atmos. Environ., 41, 4128–4137, doi:10.1016/j.atmosenv.2007.01.019, 2007.

Deutschmann, T.: Atmospheric Radiative Transfer Modelling with Monte Carlo Methods, Master's thesis, Universität Heidelberg, Germany, http://rtm.iup.uni-heidelberg.de/McArtim/, 2009.

Eck, T., Holben, B. N., Reid, J. S., Dubovik, O., Smirnov, A., O'Neill, N., Slutsker, I., and Kinne, S.: Wavelength dependence of the optical depth of biomass burning, urban, and desert dust aerosols, J. Geophys. Res., 104, 31333–31349, 1999.

Friess, U., Monks, P. S., Remedios, J. J., Rozanov, A., Sinreich, R., Wagner, T., and Platt, U.: MAX-DOAS O4 measurements: A new technique to derive information on atmospheric aerosols: 2. Modeling studies, J. Geophys. Res.-Atmos., 111, D14203, doi:10.1029/2005JD006618, 2006.

Garland, R. M., Yang, H., Schmid, O., Rose, D., Nowak, A., Achtert, P., Wiedensohler, A., Takegawa, N., Kita, K., Miyazaki, Y., Kondo, Y., Hu, M., Shao, M., Zeng, L. M., Zhang, Y. H., Andreae, M. O., and Pöschl, U.: Aerosol optical properties in a rural environment near the mega-city Guangzhou, China: implications for regional air pollution, radiative forcing and remote sensing, Atmos. Chem. Phys., 8, 5161–5186, 2008, http://www.atmos-chem-phys.net/8/5161/2008/.

Grainger, J. F. and Ring, J.: Anomalous Fraunhofer Line Profiles, Nature, 193, 762, doi:10.1038/193762a0, 1962.

Greenblatt, G. D., Orlando, J. J., Burkholder, J. B., and Ravishankara, A. R.: Absorption-Measurements of Oxygen between 330 nm and 1140 nm, J. Geophys. Res.-Atmos., 95, 18577–18582, 1990.

Hendrick, F., Van Roozendael, M., Kylling, A., Petritoli, A., Rozanov, A., Sanghavi, S., Schofield, R., von Friedeburg, C., Wagner, T., Wittrock, F., Fonteyn, D., and De Mazière, M.: Intercomparison exercise between different radiative transfer models used for the interpretation of ground-based zenith-sky and multi-axis DOAS observations, Atmos. Chem. Phys., 6, 93–108, 2006, http://www.atmos-chem-phys.net/6/93/2006/.

Hofzumahaus, A., Rohrer, F., Lu, K., Bohn, B., Brauers, T., Chang, C.-C., Fuchs, H., Holland, F., Kita, K., Kondo, Y., Li, X., Lou, S., Shao, M., Zeng, L., Wahner, A., and Zhang, Y.: Amplified Trace Gas Removal in the Troposphere, Science, 324, 1702–1704, doi:10.1126/science.1164566, 2009.

Hönninger, G. and Platt, U.: Observations of BrO and its vertical distribution during surface ozone depletion at Alert, Atmos. Environ., 36, 2481–2489, doi:10.1016/S1352-2310(02)00104-8, 2002.

Hönninger, G., von Friedeburg, C., and Platt, U.: Multi axis differential optical absorption spectroscopy (MAX-DOAS), Atmos. Chem. Phys., 4, 231–254, 2004, http://www.atmos-chem-phys.net/4/231/2004/.

Inomata, S., Tanimoto, H., Kameyama, S., Tsunogai, U., Irie, H., Kanaya, Y., and Wang, Z.: Technical Note: Determination of formaldehyde mixing ratios in air with PTR-MS: laboratory experiments and field measurements, Atmos. Chem. Phys., 8, 273–284, 2008, http://www.atmos-chem-phys.net/8/273/2008/.

Irie, H., Kanaya, Y., Akimoto, H., Iwabuchi, H., Shimizu, A., and Aoki, K.: First retrieval of tropospheric aerosol profiles using MAX-DOAS and comparison with lidar and sky radiometer measurements, Atmos. Chem. Phys., 8, 341–350, 2008, http://www.atmos-chem-phys.net/8/341/2008/.

Kraus, S. and Geyer, A.: DOASIS Jscript programming description, Institut für Umweltphysik, Universität, Heidelberg, 2001.

Kurucz, R. L., Furenlid, I., J., and Testerman, L.: Solar Flux Atlas from 296 to 1300 nm, Technical report, National Solar Observatory, 1984.

Lee, H., Irie, H., Kim, Y. J., Noh, Y., Lee, C., Kim, Y., and Chun, K. J.: Retrieval of Aerosol Extinction in the Lower Troposphere Based on UV MAX-DOAS Measurements, Aerosol Sci. Technol., 43, 502–509, doi:10.1080/02786820902769691, 2009.

Leigh, R. J., Corlett, G. K., Frieß, U., and Monks, P. S.: Spatially resolved measurements of nitrogen dioxide in an urban environment using concurrent multi-axis differential optical absorption spectroscopy, Atmos. Chem. Phys., 7, 4751–4762, 2007, http://www.atmos-chem-phys.net/7/4751/2007/.

Liu, X., Cheng, Y., Zhang, Y., Jung, J., Sugimoto, N., Chang, S.-Y., Kim, Y. J., Fan, S., and Zeng, L.: Influences of relative humidity and particle chemical composition on aerosol scattering properties during the 2006 PRD campaign, Atmos. Environ., 42, 1525–1536, doi:10.1016/j.atmosenv.2007.10.077, 2008.

Meller, R. and Moortgat, G. K.: Temperature dependence of the absorption cross sections of formaldehyde between 223 and 323 K in the wavelength range 225–375 nm, J. Geophys. Res.-Atmos., 105, 7089–7101, 2000.

Pikelnaya, O., Hurlock, S. C., Trick, S., and Stutz, J.: Intercomparison of multiaxis and long-path differential optical absorption spectroscopy measurements in the marine boundary layer, J. Geophys. Res., 112, D10S01, doi:10.1029/2006JD007727, 2007.

Platt, U. and Stutz, J.: Differential Optical Absorption Spectroscopy: Principles and Applications, Springer, Berlin, Heidelberg, Germany, 2008.

Platt, U., Marquard, L., Wagner, T., and Perner, D.: Corrections for zenith scattered light DOAS, Geophys. Res. Lett., 24, 1759–1762, 1997.

Sasano, Y.: Tropospheric aerosol extinction coefficient profiles derived from scanning lidar measurements over Tsukuba, Japan, from 1990 to 1993, Appl. Optics, 35, 4941–4952, http://www.opticsinfobase.org/abstract.cfm?URI=ao-33-30-7132, 1996.

Sinreich, R., Volkamer, R., Filsinger, F., Frieß, U., Kern, C., Platt, U., Sebastián, O., and Wagner, T.: MAX-DOAS detection of glyoxal during ICARTT 2004, Atmos. Chem. Phys., 7, 1293–1303, 2007, http://www.atmos-chem-phys.net/7/1293/2007/.

Voigt, S., Orphal, J., Bogumil, K., and Burrows, J. P.: The temperature dependence (203–293 K) of the absorption cross sections of O-3 in the 230–850 nm region measured by Fourier-transform spectroscopy, J. Photochem. Photobiol. A, 143, 1–9, 2001.

Voigt, S., Orphal, J., and Burrows, J. P.: The temperature and pressure dependence of the absorption cross-sections of NO2 in the 250–800 nm region measured by Fourier-transform spectroscopy, J. Photochem. Photobiol. A, 149, 1–7, 2002.

Wagner, T., Dix, B., von Friedeburg, C., Friess, U., Sanghavi, S., Sinreich, R., and Platt, U.: MAX-DOAS O4 measurements: A new technique to derive information on atmospheric aerosols – Principles and information content, J. Geophys. Res., 109, D22205, doi:10.1029/2004JD004904, 2004.

Wagner, T., Burrows, J. P., Deutschmann, T., Dix, B., von Friedeburg, C., Frieß, U., Hendrick, F., Heue, K.-P., Irie, H., Iwabuchi, H., Kanaya, Y., Keller, J., McLinden, C. A., Oetjen, H., Palazzi, E., Petritoli, A., Platt, U., Postylyakov, O., Pukite, J., Richter, A., van Roozendael, M., Rozanov, A., Rozanov, V., Sinreich, R., Sanghavi, S., and Wittrock, F.: Comparison of box-air-mass-factors and radiances for Multiple-Axis Differential Optical Absorption Spectroscopy (MAX-DOAS) geometries calculated from different UV/visible radiative transfer models, Atmos. Chem. Phys., 7, 1809–1833, 2007, http://www.atmos-chem-phys.net/7/1809/2007/.

Wilmouth, D. M., Hanisco, T. F., Donahue, N. M., and Anderson, J. G.: Fourier transform ultraviolet spectroscopy of the A(2)Pi(3/2)< −X(2)Pi(3/2) transition of BrO, J. Phys. Chem. A, 103, 8935–8945, 1999.

Wittrock, F., Oetjen, H., Richter, A., Fietkau, S., Medeke, T., Rozanov, A., and Burrows, J. P.: MAX-DOAS measurements of atmospheric trace gases in Ny-Ålesund – Radiative transfer studies and their application, Atmos. Chem. Phys., 4, 955–966, 2004, http://www.atmos-chem-phys.net/4/955/2004/.

Zhang, Y. H., Hu, M., Shao, M., Brauers, T., Chang, C. C., Hofzumahaus, A., Holland, F., Li, X., Lu, K., Kita, K., Kondo, Y., Nowak, A., Pöschl, U.eand Rohrer, F., Zeng, L., Wiedensohler, A., and Wahner, A.: Continuous efforts to investigate regional air pollution in the Pearl River Delta, China: PRIDE-PRD2006 campaign, Atmos. Chem. Phys. Discuss., in preparation, 2010.